Computational design of RNA-based oscillatory circuits

J. Binysh
* *University of Warwick, Complexity Department*

***Abstract*—For the synthetic biologist looking to engineer regulation of genetic circuitry, RNA is an attractive tool due to the ease of predicting its behaviour from physiochemical models. In this report, we introduce a system of ODEs to model a recently designed synthetic regulatory circuit, before attempting to estimate its unknown parameters using recent single cell time series data. We provide estimates for a subset of parameters, but find many of them to be inestimable. We discuss why this is the case for our system, and suggest how this problem might be resolved.**

I. Introduction

The process of gene expression can be summarised as follows: DNA is read, and a copy of it is made, in the form of an RNA molecule (this is called *transcription*). This RNA molecule (known as messenger RNA, or mRNA) makes its way to a piece of cellular machinery called the Ribosome, which reads it, and makes a protein - which protein is made depends on the DNA sequence originally read (*translation*).

The path from genetic transcription to protein expression is naturally regulated in many ways [1]. This regulation allows the cell to control protein expression, and so cell behaviour, in response to various environmental cues. The natural cell machinery which performs it takes the form of genetic circuits - networks of interacting gene expression regulators. This genetic circuitry offers rich possibilities for modification, and an important goal within synthetic biology is to understand and manipulate it.

As well as acting as the intermediate between DNA and protein, RNA molecules play direct and important roles in regulating gene expression [2]. For the synthetic biologist looking to engineer regulation of genetic circuitry, RNA offers an attractive alternative to more traditional methods, which typically involve using proteins to regulate DNA transcription. In comparison to proteins, it is relatively straightforward to predict the intra and intermolecular interactions of an RNA from its sequence using physiochemical models. Recently, this has been exploited to computationally design synthetic sRNAs - small RNAs which do not code for a protein, but rather have some direct regulatory function - with regulatory behaviour that can be predicted [3] [4].

This report will focus on one such sRNA system, introduced in [4]. It will extend existing understanding of it beyond the qualitative by first introducing a quantitative model of its behaviour in the form of a set of ODEs, and then fitting this ODE model to available time series data to estimate its unknown parameters.

The report is structured as follows. In the remainder of this section we review the regulatory system we will consider, and discuss recent single cell fluorescence experiments performed on it. In section II we introduce a set of ODEs to model the system. In section III we attempt to estimate its unknown parameters by fitting the model to time series data. Finally, in section IV, we conclude, and suggest directions for further work.

A. The sRNA regulatory system

In bacteria, one mechanism by which gene expression is naturally regulated is as follows [5]: In order for a bacterial mRNA to be translated into a protein, the Ribosome must initially bind to the mRNA (Fig. 1). This occurs at the Ribosome Binding Site (RBS) [6], a specific nucleotide sequence found on the mRNA.

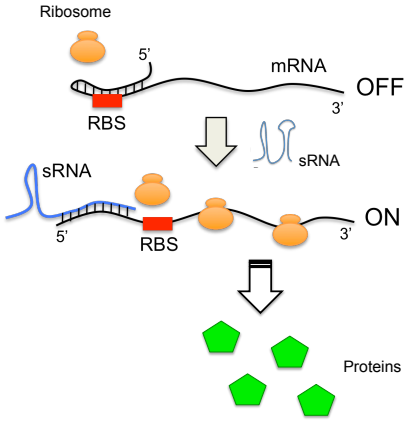

Fig. 1: A mechanism by which sRNA can regulate gene expression. Initially, the 5' UTR of the mRNA is folded over the RBS, forming a loop and blocking Ribosome binding. The sRNA binds to this loop in the mRNA, causing a conformational change which uncovers the RBS, and allows translation to occur. Image reproduced from [4].

In an mRNA there is an untranslated region of nucleotides at the 5' end of the molecule (the 5' UTR), upstream of the RBS [i]. Translation may be self repressed by this 'tail' folding over and binding across the RBS, forming a loop in the mRNA

[i] Both DNA and RNA are directional - the backbone of the molecule is not symmetric. This gives the molecule two distinct ends, denoted 5' and 3'. Translation can only occur in the 5' to 3' direction, hence the meaning of 'upstream'

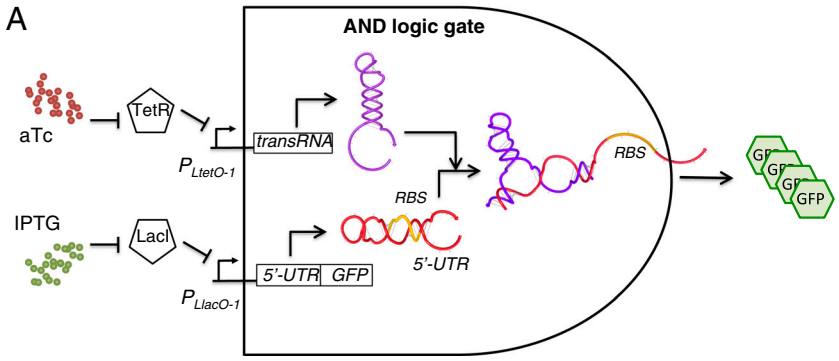

Fig. 2: A logical AND gate formed from a self repressed mRNA, and an sRNA which uncovers its RBS. In this system, transcription of the sRNA (transRNA) and mRNA (5'-UTR,GFP) are controlled by two promoters, $P_{\mathrm{LtetO-1}}$ and $P_{\mathrm{LlacO-1}}$. These are disabled by the presence of two chemical repressors, TetR and LacI, found naturally in the strain of *E. coli* discussed. These chemical repressors are themselves disabled by two chemicals, aTC and IPTG. In the notation of the diagram, a barred line indicates repression, and an arrowed line indicates production. We see a 'double negative' in aTc repressing TetR, which itself represses transcription of the sRNA (likewise for IPTG and the mRNA). Thus the presence of the sRNA and mRNA are controlled by the presence of aTc and IPTG, which can be experimentally introduced to the cell. Image reproduced from [4].

and preventing the Ribosome from binding (Fig. 1). This self repression may be released with an sRNA which binds to this looped tail - the new conformation of the sRNA:mRNA complex uncovers the RBS, allowing the Ribosome to bind. In summary, the presence of the sRNA positively regulates gene expresssion.

[4] proposed a computational methodology to design general genetic circuits based on RNA interactions, and as a case study of the methodology chose to design a synthetic sRNA-mRNA pair capable of acting in the manner described above. The algorithm assumed an interaction scheme between the RNA's as shown in Fig. 3. The sRNA and mRNA, originally in their own individually folded states, would initially interact via a small 'toehold' sequence of unpaired nucleotides to form an unstable transition state. This intermediate complex would then rapidly form a final, stable complex with the desired conformation. By finding sRNA and mRNA sequences which optimised the energy landscape shown in Fig. 3, [4] suggested several sRNA-mRNA pairs which would work in tandem to form a stable hybrid with the RBS free.

The authors then experimentally validated their methodology by testing the suggested sRNA-mRNA pairs in *E. coli* bacteria. Further, by placing the *in vivo* concentrations of the sRNA and mRNA under the control of tuneable promoters [ii], they constructed a logical AND gate from one of the proposed pairs (Fig. 2).

In this system, transcription of the DNA sequences which produce the designed sRNA and mRNA are placed under the control of promoters, $P_{\mathrm{LtetO-1}}$ and $P_{\mathrm{LlacO-1}}$ [7]. These are in turn controlled by two transcriptional repressors, TetR and

[ii] A promoter in a DNA sequence is a sequence of nucleotides, found upstream of where transcription of a gene begins, which can influence the transcription rate of the gene.

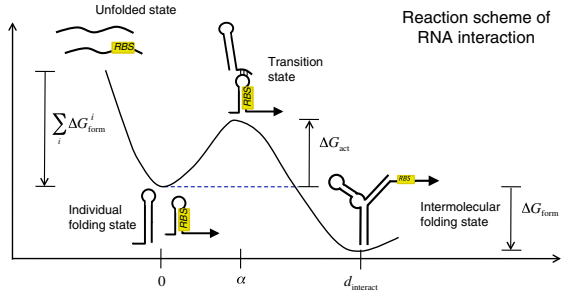

Fig. 3: The reaction scheme between the synthetic sRNA-mRNA pairs designed in [4]. The reaction co-ordinate is defined as the number of paired nucleotides, and the vertical axis denotes free energy. The RNA's initially interact via a small 'toehold' sequence, forming an unstable transition state, which then stabilises to give the final compound. Image reproduced from [4]

LacI respectively, which are naturally present in the strain of *E. coli* used. These repressors disable the promoters, and so by default transcription of both RNA's is turned off, and no protein is produced. These repressors can themselves be disabled by the presence of two chemicals, aTc and IPTG, which can be introduced externally into the cell (Fig. 2). So transcription of the two RNAs is indirectly controlled by the presence of aTc and IPTG - if neither is present, sRNA and mRNA transcription is repressed, and no protein is produced. If only one is present, the AND gate remains off, either because there is no mRNA to be translated into protein, or because the mRNA is self repressed. But when both are present, both sRNA and mRNA are produced, the conformational change in the mRNA discussed above occurs, and protein is produced.

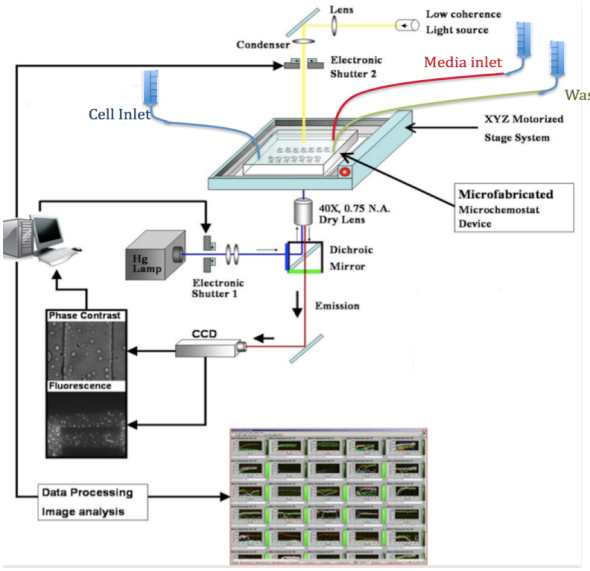

Adapted from Balagadde, 2007

Fig. 4: An overview of the experimental setup which allows single cell fluorescences to be recorded over time. Shown are the bacterial growth chambers (labelled 'Microfabricated Microchemstat device'), the microscope imaging them (the surrounding apparatus - lens, condenser, Dichroic mirror, CCD etc.), and the software constructing fluorescence time series. Image reproduced from [8].

Although a qualitative understanding of this system exists [4], it is of interest to attempt a quantitative understanding of the genetic circuit involved. Such an understanding would allow, for example, tailoring of the system in response to design requirements, by altering the values of the important parameters of the model. By changing which sRNA-mRNA pair is used in the system, it would also allow exploration of the relationship between the thermodynamic properties of each device, and any rate constants in the proposed model.

B. Single Cell Fluorescence Data

mRNA concentrations in the system shown in Fig. 2 can be indirectly observed by designing the mRNA to code for green fluorescent protein (GFP) [iii]. Recent experiments have used timelapse microscopy to observe the fluoresence of *E. coli* bacteria which contain the above sRNA-mRNA pair, as they are periodically forced with a varying aTc or IPTG concentration [8].

The experimental setup is as follows (Figs. 4, 5): A single layer of the bacteria are grown in rows of chambers. A medium constantly flows through these chambers, allowing normal feeding of the bacteria, and the introduction of aTc or IPTG. The chambers are monitored with software which traces the position of each cell over time, allowing time series of individual cell fluorescences to be recorded.

The data we will consider consists of two sets of individual cell time series, labelled *13_9* and *14_7* [9]. They correspond

[iii]The methodology of [4] only optimises the 5' UTR of the mRNA, so the actual protein being coded for is unimportant.

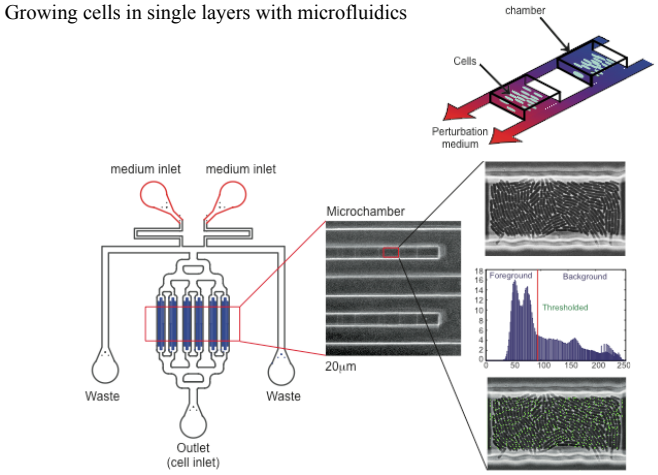

Fig. 5: A diagram of the bacterial growth chambers shown in Fig. 4. The schematic shows the chambers themselves, and the medium inlet where aTc and IPTG are let in. Shown also are photographs of a row of chambers, and an individual chamber with bacteria growing in it. Image reproduced from [8].

to different experimental runs of the above apparatus, for which IPTG concentration was held constant, at a value assumed large enough to saturate the cell's response (i.e the IPTG input to the AND gate is always 1), and aTc concentrations were varied periodically. Appendix A shows the full datasets, with their forcing functions. Note that *13_9* contains two different forcing periods.

II. ODE Model

In eq. (1) - eq. (7), we present a modified version an existing model which describes the system [9], consisting of a set of ODE's with mass action kinetics [10]. Its state is given by the vector $(s, m, s:m, c, p, g, z)$, with all other variables representing model parameters. Tables I and II give complete descriptions of the parameters and state variables.

$$\frac{ds}{dt} = \frac{N\alpha_T}{f_T}y(t) - (\mu + \delta_s)s - k_{\text{on}}sm + k_{\text{off}}s:m \quad (1)$$

$$\frac{dm}{dt} = \frac{N\alpha_L}{f_L}x(t) - (\mu + \delta_m)m - k_{\text{on}}sm + k_{\text{off}}s:m \quad (2)$$

$$\frac{ds:m}{dt} = k_{\text{on}}sm - (k_{\text{off}} + k_{\text{hyb}})s:m - (\mu + \delta_{sm})s:m \quad (3)$$

$$\frac{dc}{dt} = k_{\text{hyb}}s:m - (\mu + \delta_c)c \quad (4)$$

$$\frac{dp}{dt} = \beta m + f_s\beta c - (\gamma + \mu + \delta_g)p - \frac{v_z p}{K_z + p + g} \quad (5)$$

$$\frac{dg}{dt} = \gamma p - (\mu + \delta_g)g - \frac{v_z g}{K_z + p + g} \quad (6)$$

$$z = z_0 + \frac{g}{\Theta} \quad (7)$$

Based on the reaction mechanism in Fig. 3, the hybridization of the sRNA and mRNA first into an unstable complex, then a

stable one, is modelled in eq. (1) - eq. (4). The initial binding is modelled as a reversible reaction with forward and backward rates k_{on} and k_{off}:

$$\text{sRNA} + \text{mRNA} \underset{k_{\text{off}}}{\overset{k_{\text{on}}}{\rightleftharpoons}} \text{sRNA} : \text{mRNA}_{\text{unstable}},$$

after which the stabilization is modelled as an irreversible reaction with rate k_{hyb}:

$$\text{sRNA} : \text{mRNA}_{\text{unstable}} \xrightarrow{k_{\text{hyb}}} \text{sRNA} : \text{mRNA}_{\text{stable}}.$$

In addition, these complexes are given degradation rates, δ_s, δ_m, δ_{sm}, δ_c, and dilutions of chemical concentrations due to cell growth are modelled with a dilution rate μ.

Control of the system by aTc is modelled by $y(t)$ in eq. (1). This function models the response of the sRNA transcription rate to (time varying) aTc concentration - it is normalised to lie between 1 and f_T, and is typically sigmoid in response to aTc concentration [4]. α_T is the maximal transcription rate of the $P_{\text{LtetO}-1}$ promoter, and N is the copy number, which models the fact that when engineering the system, many copies of the $P_{\text{LtetO}-1}$ promoter may be placed in the bacterial DNA. Thus the transcription rate varies as a sigmoid bounded by $N\frac{1}{f_T}$ and $N\frac{\alpha_T}{f}$ in response to aTc concentration. Identical considerations hold for $x(t)$ in eq. (2), and IPTG concentration.

We explicitly model translation as a simple one step process in eq. (5) - eq. (7). There is a small rate of translation of the self repressed mRNA [4], which is modelled at rate β, and a larger one for translation of the stable complex, βf_s. Here f_s represents the fractional change in translation rate between the repressed mRNA and the unrepressed complex:

$$\text{sRNA} : \text{mRNA}_{\text{Stable}} \xrightarrow{\beta f_s} \text{GFP}_{\text{Immature}},$$

$$\text{mRNA} \xrightarrow{\beta} \text{GFP}_{\text{Immature}}.$$

Initially, the translated GFP is in an immature state, and will not fluoresce. To account for this, we include a maturation rate, γ:

$$\text{GFP}_{\text{Immature}} \xrightarrow{\gamma} \text{GFP}_{\text{Mature}}.$$

Degradation of the immature and mature GFP is modelled in two ways. Firstly a generic degradation rate δ_g is included, assumed identical for the mature and immature species, along with the dilution rate μ shared by all species. Secondly, in the experimental setup we can arrange for GFP molecules to be produced with a *degradation tag* attached to them [11]. This tag is identified by an enzyme, ClpX, which will then degrade the molecule the tag is attached to. This degradation process is modelled by the final terms in eq. (5) and eq. (6). Finally, eq. (7) represents calibration of mature GFP levels to experimentally observed fluorescence, assuming a linear response.

TABLE I: State Variables

State variable	Units	**Definition**
s	nM	sRNA concentration
m	nM	mRNA concentration
$s:m$	nM	Unstable sRNA:mRNA complex concentration
c	nM	Stable sRNA:mRNA complex concentration
p	nM	Immature GFP concentration
g	nm	Mature GFP concentration
z	Arbitrary (AFU)	Observed fluorescence
$y(t)$		Unitless aTc forcing function
$x(t)$		Unitless IPTG forcing function

TABLE II: Model Parameters (those to be estimated shown in bold)

Parameter	**Units**	**Definition**
N		Number of copies of promoter existing on plasmid DNA
z_0	Arbitrary (AFU)	Baseline experimental fluorescence
α_L	nM/min	Maximal transcription rate of $P_{\text{LlacO}-1}$ promoter
α_T	nM/min	Maximal transcription rate of $P_{\text{LtetO}-1}$ promoter
f_L		Unitless ratio between repressed and unrepressed $P_{\text{LlacO}-1}$ transcription rate
f_T		Unitless ratio between repressed and unrepressed $P_{\text{LtetO}-1}$ transcription rate
δ_g	/min	GFP degradation rate
γ	/min	GFP maturation rate
v_z	nM/min	Degradation constant of clpx
K_z	nM/min	Dissociation constant of clpx
$\boldsymbol{\Theta}$	nM/AFU	Ratio between GFP concentration and observed fluoresence
$\boldsymbol{\mu}$	/min	Dilution rate
$\boldsymbol{\delta_m}$	/min	mRNA degredation rate
$\boldsymbol{\delta_s}$	/min	sRNA degredation rate
δ_{sm}	/min	Unstable sRNA:mRNA degradation rate
δ_c	/min	Stable sRNA:mRNA degradation rate
$\boldsymbol{k_{on}}$	/min	sRNA:mRNA binding rate
$\boldsymbol{k_{off}}$	/min	sRNA:mRNA unbinding rate
$\boldsymbol{k_{hyb}}$	/min	sRNA:mRNA hybridization rate
$\boldsymbol{\beta}$	/min	Baseline translation rate of repressed mRNA
$\boldsymbol{f_s}$		Ratio of repressed mRNA to unrepressed complex translation rate.

III. Parameter Estimation

Our next goal is to estimate the unknown parameters of this model, given the available fluorescence time series data, by fitting the predicted time series from the model to the data. Typically, this is done by minimising the least squares error between model prediction and the experimental data [12]–[14]. Suppose we have some ODE model of our system

$$\frac{\mathrm{d}\mathbf{y}}{\mathrm{d}t} = \mathbf{f}(\mathbf{y}, \boldsymbol{\theta}, t), \tag{8}$$

where $\mathbf{y}$ is our state vector, $\boldsymbol{\theta}$ is a vector of model parameters, and t is time. The model may be integrated numerically, giving a prediction $\mathbf{y}(t, \boldsymbol{\theta})$. The least squares error between the model

prediction and an experimental time series is defined as

$$\sum_{i=1}^{n}(\mathbf{y}_{\exp}(t_i) - \mathbf{y}(t_i, \boldsymbol{\theta}))^2, \tag{9}$$

where the experimental time series, $\mathbf{y}_{\exp}(t_i)$ is recorded at timepoints t_i, $i = 1 \ldots n$. This error function defines a landscape in $\boldsymbol{\theta}$ space, and we seek to minimise it by varying $\boldsymbol{\theta}$. In our case, we do not have experimental data on the full state vector, but only one component of it - the observed fluorescence, $z(t)$. In addition, rather than a single experimental run, we have many, corresponding to a time series from each cell. We incorporate this by fitting to the experimental mean of the data, and only minimising over the observed component. Our minimisation problem is thus

$$\arg\min_{\boldsymbol{\theta}} \sum_{i=1}^{n}(z_{\exp,\mathrm{mean}}(t_i) - z(t_i, \boldsymbol{\theta}))^2. \tag{10}$$

The next step is performing the minimisation. In general, the landscape defined by the error function may be rugged and contain many local minima, which a local optimisation algorithm may get stuck in. To try and surmount this problem, [13] suggests the use of a global optimisation algorithm, and in particular demonstrates that several Evolutionary Algorithms perform well on a test problem involving a set of ODEs modelling a biological system. We choose one of those recommended, the CMA-ES [15], [16], which in addition.

why use CMA-ES? Some refs

In order to reduce the dimensionality of our search space, we can perform a literature search for existing values of some of our parameters, simplify our model to remove others, and place bounds on those that remain. Appendix B contains a list of parameter values found in the literature, where available, and their reference, as well as initial bounds placed on parameters not found in the literature. To further reduce the search space, we simplify the model by assuming that δ_m, δ_{sm} and δ_c all take similar values, and set them equal. After this is done, we are left with a 9 dimensional search space, bounded by a hypercube (parameters to be estimated are shown in bold in table II).

A. Initial Parameter Estimates

We begin by fitting the two datasets individually, by choosing 200 sets of the parameters uniformly distributed over our initial parameter bounds, and running the CMA-ES starting from them. Results are shown in Figs. 6, C.1. Figs. 6a, 6b demonstrate that the model is capable of quantitatively capturing the data. However, histograms of the parameter estimates (Figs. 6c, 6d) indicate that many are not tightly constrained, taking values right across the initial bounding range specified - in particular, k_{off}, δ_m and δ_s are very weakly constrained, with substantial numbers of runs constrained only by the initial bounding box. By contrast, some parameter estimates (μ in particular) are much tighter. Θ appears tightly constrained, but many of the estimated values are close to the upper bound set, and must be treated with caution. We also note a shift in the estimated value of μ between the two datasets. Since the two sets of estimates for μ are relatively sharp, this variation may be a genuine feature of the data - one explanation for it is a variation in cell growth rate between the two experimental runs [14].

Figs. C.1a, C.1b show correlation matrices between parameter sets[iv]. These correlation matrices indicate that there are spaces of parameters within which the fitness function remains approximately constant - for example, in both datasets there exists a positive correlation between values of μ and β. Referring to eq. (5), this makes heuristic sense - the two parameters may have similar effects on model predictions, and may be able to co-vary in such a way as to leave the model prediction unchanged. The results suggest a fitness landscape relatively flat to perturbations in certain combinations of parameters, and indicate we may have difficulty obtaining unique estimates of the model parameters.

We can test the predictive ability of our model by cross validating, either by taking the parameter values found in the fitting of one dataset and using them to give model predictions for another, or only fitting part of a single dataset and predicting the rest. We begin by fitting to only the data for the first forcing period in *13_9*, and then predicting the full time series. Results are shown in Fig. 7a, for the parameter set giving the lowest error on the training data. We see the prediction is very similar to that obtained by fitting to the full dataset (Fig. 6a). Next, we take the parameter values giving the best fit for the *13_9* dataset and use them to predict the *14_7* dataset, and vice versa. Results are shown in Figs. 7b, 7c. Though the predictions are reasonable, they are substantially worse than the predictions for the data they were trained on. One reason for this may be the variation in parameter values between experiments suggested above. We can also fit to both datasets combined, by extending eq. (10) to a sum over multiple datasets. Results are shown in Appendix D. We are unable to achieve error values as low as those found when fitting individual datasets. In addition, we do not see a tightening of the estimates on our parameters, as we might expect from including the additional data. Instead, many parameter estimates remain spread across the initial bounding region.

Taken together, these results suggest that simply performing a least squares fit on the available data will not give unique estimates for many of the parameters. In the following sections we investigate this further.

B. Parameter Estimability

There are two main reasons why a parameter may not be estimable [17]–[21]: Model predictions may be insensitive to the value of a particular parameter, or the effects of varying one parameter on model predictions may be highly correlated with the effects of varying several others.

[iv] These are computed by viewing each of the estimated parameter sets as a sample from a multivariate random variable. An element of the correlation matrix R_{ij} is then the Pearson correlation coefficient between the i^{th} and j^{th} random variable - or, in our case, the i^{th} and j^{th} parameters

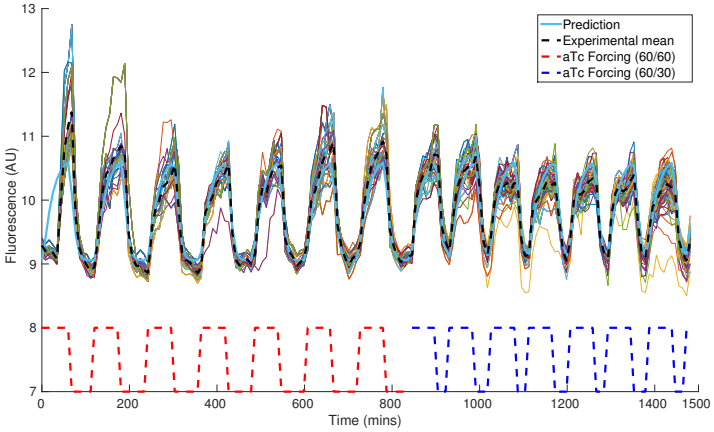

(a) Model prediction, using the parameter set with the smallest error value of the initial 200 found, for the *13_9* dataset.

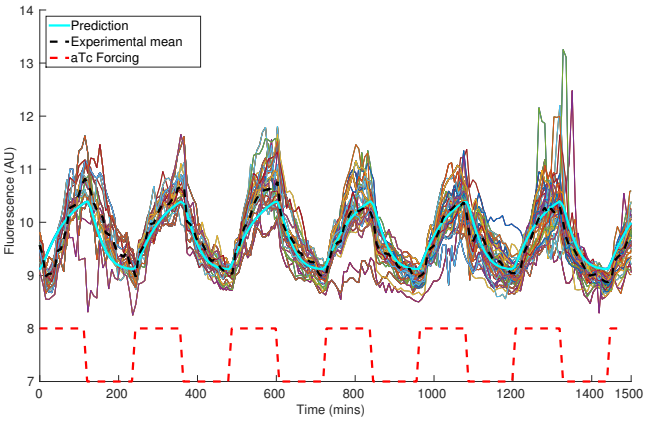

(b) Model prediction, using the parameter set with the smallest error value of the initial 200 found, for the *14_7* dataset.

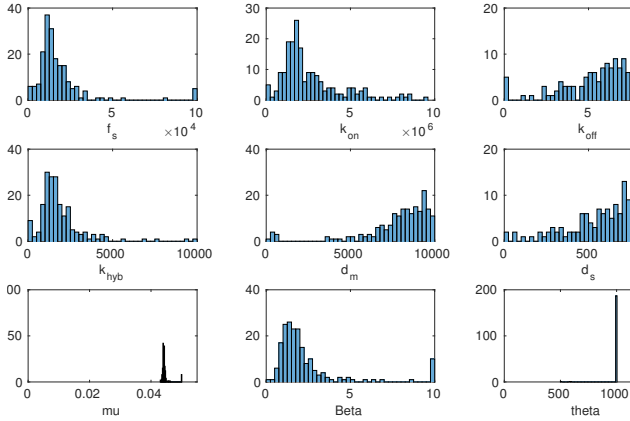

(c) Histogram of estimated parameter values, found from 200 runs of the CMA-ES algorithm. Fitted to the *13_9* dataset.

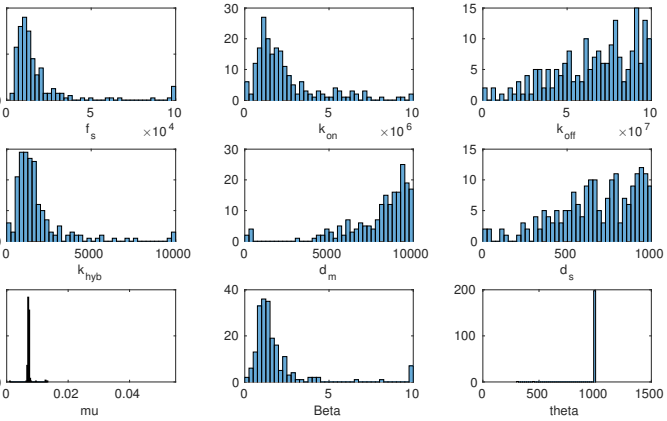

(d) Histogram of estimated parameter values, found from 200 runs of the CMA-ES algorithm. Fitted to the *14_7* dataset.

Fig. 6: Parameter estimates and model predictions for the *13_9* and *14_7* datasets. Note that in the model predictions, aTc forcing is shown - IPTG concentration is constant at a level which saturates the cell's response. The forcing curve's height is schematic - aTc concentration is switched between off and on (where by 'on' we mean a level which saturates the cell's response).

These problems may stem from structural inadequacies in the model (often termed *structural identifiability*), in which two different parameter sets can give identical model predictions [20], [21]. If this is the case, no amount of experimental data will allow us to estimate parameters, and we must consider reformulating the model[v]. Problems may also arise for more practical reasons (*practical identifiability* [17]). For example, it is possible that in the experimental regime we operate in (eg. the forcing function we use, the components of the model's state we can observe), parameter effects may be weak, or highly correlated, but in other regimes this is not true. In this case, parameter estimates may be improved by taking data in more varied experimental conditions, or attempting to increase the number of model outputs observed - in our case, observing more of the state vector than simply z.

We may begin to investigate these issues in our model by performing a local sensitivity analysis about one of the solutions found in our initial parameter estimation. We numerically estimate the sensitivity matrix, S:

$$S_{ij} = \hat{\theta}_j \frac{\partial z}{\partial \theta_j}\bigg|_{t_i}, \tag{11}$$

where S_{ij} is the derivative of the observed fluorescence, $z(t)$,

[v] A simple example of a structurally non - identifiable model is $y = \beta_1\beta_2 x$, where we are given data (x, y), and asked to estimate parameters β_1 and β_2 - we can see that, in principle, only the product $\beta_1\beta_2$ can ever be estimated, a problem no amount of data can fix.

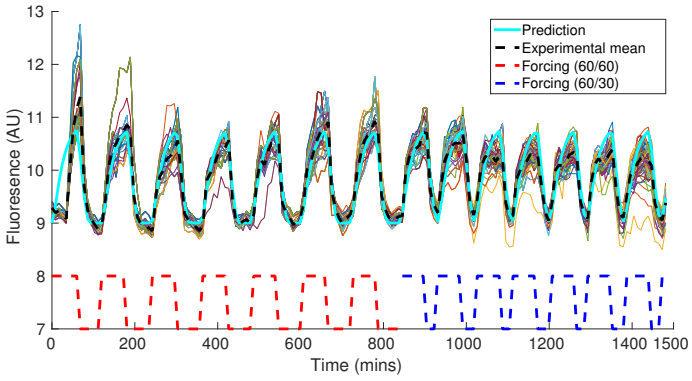

(a) Model trained on *13_9* 60/60 data only, full prediction

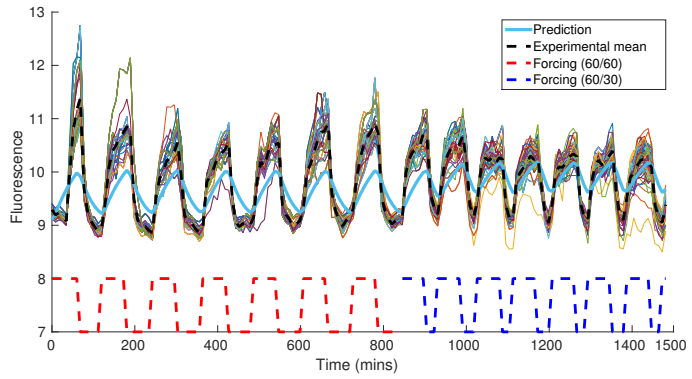

(b) *14_7* prediction *13_9* data

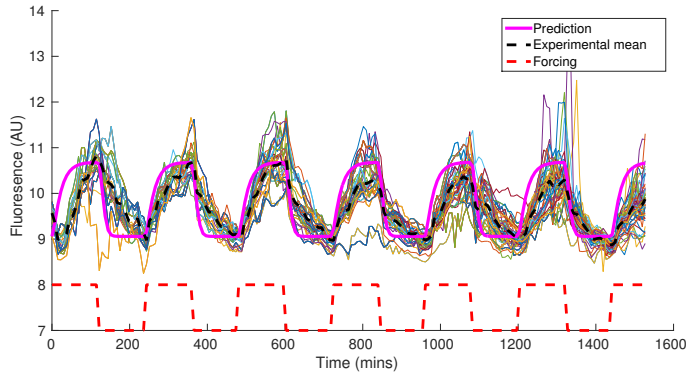

(c) *13_9* prediction *14_7* data

Fig. 7: Cross validating data by taking parameter estimates from one dataset, and using them to predict another. 7a shows model predictions for the full *13_9* dataset, when only trained on the first forcing period data. 7b, 7c show model predictions for fitting to one dataset, and predicting the other.

with parameter θ_j, evaluated at timepoint t_i. Each column of S is a time series of sensitivity co-efficients, which describe how sensitive z is to perturbations in the parameter associated with that column, and at what times it is most sensitive. $\hat{\theta}_j$ is the value of the parameter that the derivative is being evaluated at. It is included to set the scale that parameters may vary at, to ensure that apparently small sensitivity values do not result from a poor choice of units.

Suppose we take a set of parameters that give a local minima in the error function, and plot the sensitivity curves (columns of S) over the range of observation times. It can be shown that, if two curves are linearly dependent, there exists a degenerate line of minima in parameter space, and the two associated parameters cannot be simultaneously estimated [19]. Related to this fact, a number of measures have been proposed to assess parameter estimability from the sensitivity matrix [17], the simplest of which is to plot the sensitivity curves as a function of time, and visually check for obvious linear relations between them.

Fig. 8 shows plots of each column of S, evaluated at the parameter set giving the lowest error in the *13_9* dataset (Fig 6a). Fig. 8a shows them unscaled, Fig. 8b shows them scaled by the norm of each column of S, so that their shapes may be more easily compared.

We see that many of the parameters give sensitivity curves of similar shapes, and have near linear dependence - this implies that the effects of perturbing any one of these parameters all look similar in terms of model output, and are hard to distinguish between. This may help to explain why some of our initial parameter estimates are very loose, and why there are correlations between the estimated parameter sets - this result suggests there is a family of parameters all of which, in terms of the model output we have available, cannot be resolved. As such, we should view estimates of these parameters with extreme caution. Note that the sensitivity curve that looks least similar to the others in Fig. 8b - μ - corresponds to a relatively tightly estimated value in Fig. 6. Note also that the curve for Θ is very similar to those for the remaining parameters. This suggests that our estimated value of Θ in Fig. 6c is misleading, and likely a consequence of the initial bounding box.

C. Differing timescales within the system

Fig. 9 shows model output for all state variables, using the parameter values giving the lowest error on the *13_9* dataset, and normalised to lie on the same scale. We see that $s, m, s:m$ and c respond rapidly to the forcing function, flipping between the two fixed points defined by the step function forcing almost instantly. By contrast, there is delay in the response of p and g, on a timescale comparable to the period of the forcing. This result suggests that, at least in some of the parameter sets initially estimated, the system may have two timescales in it - a fast timescale in which eq. (1) - eq. (4), representing the hybridization of the sRNA and mRNA into a stable complex, equilibrate in response to external forcing, and a slower timescale, in eq. (5), eq. (6), in which measured fluorescence changes in response to the forcing. Biologically, this would correspond to eq. (5), representing translation, being a rate limiting step.

If this is the case, then our experimental data can only probe the system via the fixed point of eq. (1) - eq. (4), whose value is communicated to the rest of the model via the $\beta m + f_s \beta c$

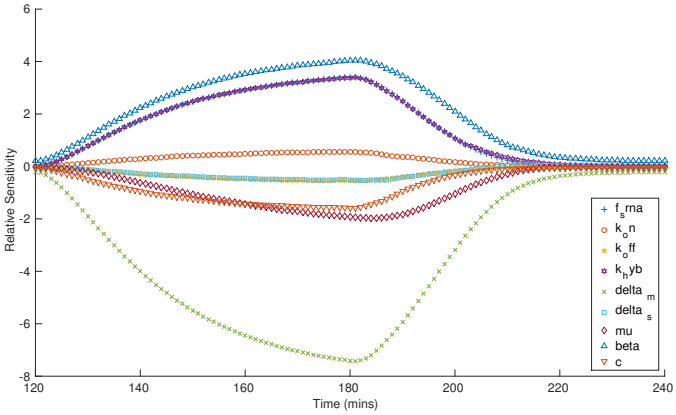

(a) Unscaled

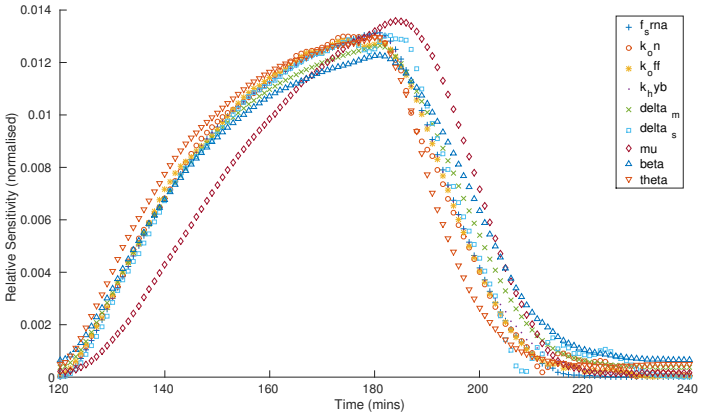

(b) Scaled

Fig. 8: Sensitivity coefficients S_{ij} eq. (11), evaluated about a set of estimated parameters from the *13_9* dataset, for a single oscillation. 8a shows them unscaled, 8b shows them scaled by the norm of each column of S.

term in eq. (5) [vi]. $\beta m + f_s\beta c$ will flip between two values, which will cause the fixed point values of p and g to flip, with p and g tending towards them in response. This is what we observe in Fig 9.

This would explain the similarity between the sensitivity curves of many parameters - if the parameters in eq. (1) - eq. (4) can only act to alter the fixed point values of p and g which the system tends toward, they all play qualitatively identical roles on the time series of z. The fact that $\beta m + f_s\beta c$ is the only term in eq. (5), eq. (6) to include f_s and β may also explain the similarity of the sensitivity curves for these parameters to those found in eq. (1) - eq. (4) (Fig. 8b), by the same reasoning. This explanation also suggests that all parameter sets giving the same value of the model's fixed point will give similar model predictions - and there may be

[vi] Explicit forms for m and c are given in appendix E

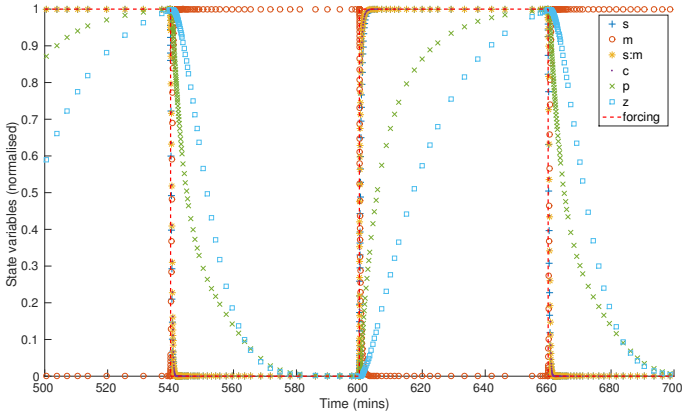

Fig. 9: Model output for all state variables over two oscillations, using the parameter values giving the lowest error on the *13_9* dataset, and normalised to lie on the same scale. Note g is not explicitly shown, but is simply a rescaling of z and as such would lie over it.

many, very different, parameter sets which all give the same fixed point. Fig. F.1 shows a scatterplot of error function value against $\beta m + f_s\beta c$ for the 200 estimated parameter sets for the *13_9* dataset, and demonstrates that, although individual parameter values can be spread across very large ranges, they are correlated in such a way as to give similar model fixed points.

D. A simplified model

These results suggest we may simplify our model, by replacing $\beta m + f_s\beta c$ in eq. (5) with the forcing function used in eq. (1), and removing eq. (1) - eq. (4) entirely - in other words, moving the forcing term directly to the translation step. The simplified model is shown in eq. (12) - eq. (14):

$$\frac{dp}{dt} = Fy(t) - (\gamma + \mu + \delta_g)p - \frac{v_z p}{K_z + p + g} \tag{12}$$

$$\frac{dg}{dt} = \gamma p - (\mu + \delta_g)g - \frac{v_z g}{K_z + p + g} \tag{13}$$

$$z = z_0 + \frac{g}{\Theta} \tag{14}$$

where F is a phenomenological scaling factor, and $y(t)$ is the same forcing function used in eq. (1). We now have three free parameters, F, μ, Θ, which we may estimate as before. Based on the results of earlier fitting, we set a new bounding box for these parameters (shown in table IV) and run the CMA-ES 400 times. Results are shown in Fig. 10, for the *13_9* dataset only.

In contrast to the results of Fig. 6, we see relatively tightly estimated parameters, with no estimated values near the initial bounding box. Further, this simplified model achieves error values as low as the more complex model. Fig G.1 shows that the simplified algorithm is more consistently able to find the minimal function value identified in Fig. C.1c, possibly

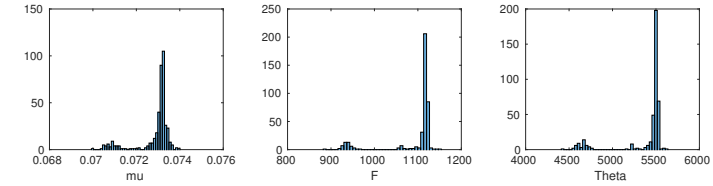

(a) Histograms of estimated parameter values, using the simplified model eq. (12) - eq. (14).

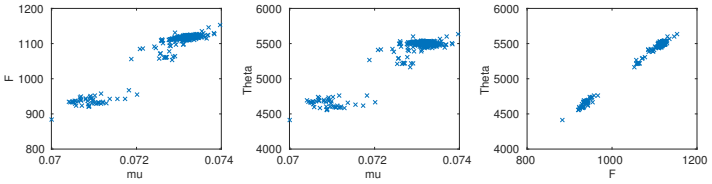

(b) Scatterplots of estimated parameters shown in 10a against one another

Fig. 10: Histograms and scatterplots of parameter estimates, found using the simplified model eq. (12) - eq. (14).

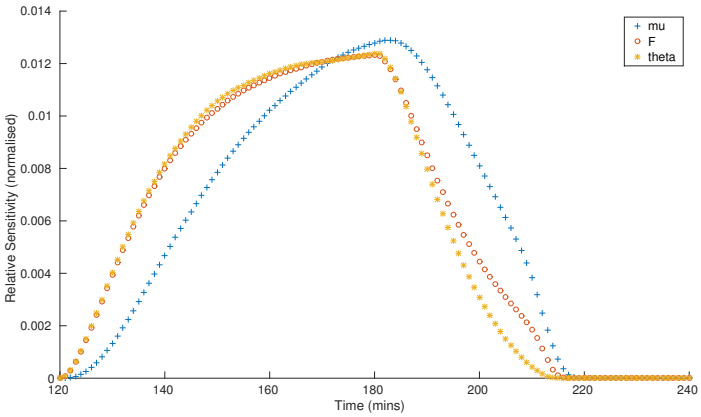

Fig. 11: Using the simplified model eq. (12) - eq. (14), normalised sensitivity coefficients S_{ij} evaluated about a set of estimated parameters from the *13_9* dataset, for a single oscillation.

because the low dimension of the new model makes parameter space easier to search.

We note that 10b shows a strong positive correlation between the minima found for F and Θ. This is consistent with the normalised sensitivity curves for the *13_9* dataset, shown in Fig. 11. As before, the similarity of the F and Θ curves suggests that any minima in $F - \Theta$ space will be locally non-unique [19]. This may be explained as follows: neglecting the ClpX degradation term, eq. (12) is a simple exponential decay to a fixed value. Here, F will determine the value the p will tend to, and μ will determine its rate constant. F is then a linear scaling factor, just as Θ is - both scale the value the exponential will tend to.

We also note that the parameter estimates come in two distinct clusters. We further investigate by fixing the value of Θ, and plotting the error as a function of μ and F. Results are shown in Fig. 12. We find a local basin in $\mu - F$ space, pocketed by many local minima of similar fitness values. The optimisation algorithm will always terminate in one of these local minima, explaining the disconnected clusters shown in Fig. 10b. Thus the tightness of each peak in Fig. 10a is misleading - the uncertainty in parameter estimates is better reflected by the contours of Fig. 12b.

IV. Conclusions and Further work

In this report, we have presented a system of ODE's to model a recently proposed synthetic RNA regulatory circuit [4], and attempted to estimate the model's parameters using existing time series data, with a least squares minimisation approach similar to that found in recent synthetic biology literature [14]. We have found many of the parameters contained in the full model to be inestimable, and suggested reasons for why this might be. We have further suggested a simplified model, which provides an equally good description of the data with fewer parameters than the initial model.

The results in this paper demonstrate that, even though the original model has a solid biological rationale, some parameters included in it may not be estimable. The suggested reason for this is that eq. (5) represents a rate limiting step, and so the parameters in eq. (1) - eq. (4) only work to alter the fixed point value of $\beta m + f_s \beta c$ in eq. (5), causing them to give qualitatively identical effects on model predictions. A simplified model, consisting of three free parameters, gives model predictions with errors as low as the full model, but contains parameters which can be estimated unambiguously.

These results suggest that if estimates of the parameters contained in eq. (1) - eq. (4) are desired, fluorescence time series data alone will not be sufficient, and new experiments are needed. If possible, direct observations of other components of the state vector - s, m, $s:m$ and c - would improve parameter estimates by giving access to the 'fast' timescale. Another option would be further investigation of the methods presented in [17], [18], [22]. Given a complex chemical model based on physical principles, and limited data, these methods rank parameters in order of estimability, and can determine if a subset of parameters might be estimable.

On the other hand, if a good description of the fluorescence data is what is really of interest, the simplified model may be a better starting point. On the experimental side, μ and Θ are both parameters which can be easily estimated independent of our datasets - a realistic range of values could be used to bound the error function profile shown in Fig. 12. Further modelling work may focus on improving the modelling of translation, the rate limiting step - [14], for example, uses a more detailed model than our single step description of translation. Any additional parameters introduced will likely act on the same timescale as μ, and stand a better chance of being estimable.

Further work may also consist of fitting each timeseries individually, rather than fitting to the experimental mean, as

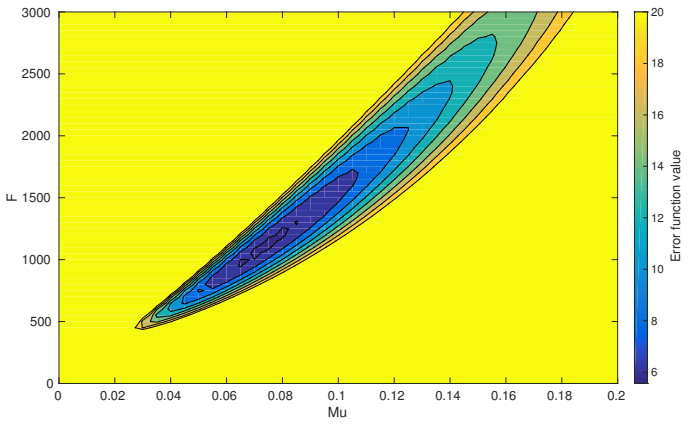

(a) A basin of low error values in $\mu - F$ space. Note the colour scaling maps all values above 20 to the maximum colour.

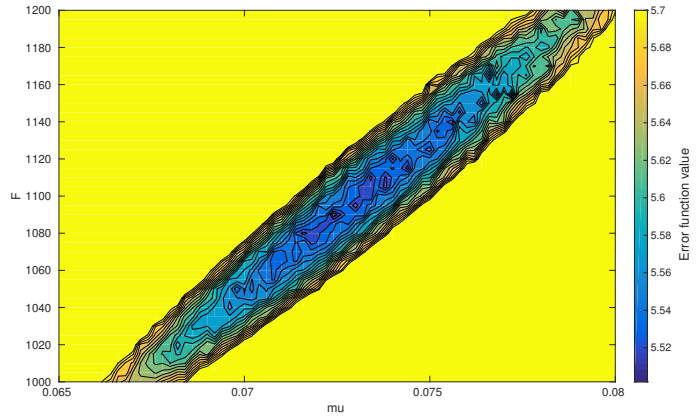

(b) Zoomed in on the bottom of the basin in Fig.12a. Note the colour scaling maps all values above 5.7 to the maximum colour.

Fig. 12: Error function plotted as a function of μ and F, $\Theta = 5400$ (the modal value of Θ in Fig. 10a). Note the many disconnected local minima in the bottom of a basin of low error function values.

described in eq. (10). This would allow us to detect cell to cell variability in parameter values within each dataset, something we have already suggested possible between datasets.

We may also consider changing our methodology for parameter estimation. Using a least squares minimisation approach has several problems, the first of which is local minima. Using the CMA-ES will give better results than a local minimisation algorithm, but one can never be sure that a global optimum has been found - for example, [13] compares several algorithms and finds, in the test case considered, none locate the true global optimum. A related problem is that of working with point estimates of parameters rather than distributions. The CMA-ES will only ever find a single optimum, giving a point estimate of parameter values, with no uncertainty information. To surmount this problem, we may rerun the algorithm many times, from many starting locations, and interpret the resulting spread of parameter values found as an uncertainty [14], as we have done in this report. However this methodology is rather ad hoc, and we have seen in Fig. 12 that it can give a misleading impression of how tightly estimated parameters are.

Another approach might be to use Markov Chain Monte Carlo (MCMC) to perform a Bayesian parameter estimation [23], [24]. This method would explicitly provide us with marginal distributions of parameter probabilities, giving a more complete picture of the best parameter sets and their uncertainties than we currently have - we would still be able to pick out a maximum likelihood point estimator, as we do now, but rather than getting an ad hoc picture of the uncertainty in the parameters by repeatedly running the minimisation algorithm, the marginals would give us this information directly. However, this change in methodology would not have allowed us to gain estimates of the parameters in the original model, and is not necessary for the simplified one. It may be useful to use in place of the least squares approach if further modelling of the translation step is pursued.

REFERENCES

[1] B. Alberts, A. Johnson, J. Lewis, M. Raff, K. Roberts, and P. Walter., *Molecular Biology of the Cell*, 4th ed. Garland Science, 2002.

[2] F. J. Isaacs, D. J. Dwyer, and J. J. Collins, "RNA synthetic biology." *Nature biotechnology*, vol. 24, no. 5, pp. 545–554, 2006.

[3] G. Rodrigo, T. E. Landrain, S. Shen, and A. Jaramillo, "A new frontier in synthetic biology: Automated design of small RNA devices in bacteria," pp. 529–536, 2013.

[4] G. Rodrigo, T. E. Landrain, and A. Jaramillo, "De novo automated design of small RNA circuits for engineering synthetic riboregulation in living cells," *Proceedings of the National Academy of Sciences*, vol. 109, no. 38, pp. 15 271–15 276, 2012.

[5] T. Soper, P. Mandin, N. Majdalani, S. Gottesman, and S. a. Woodson, "Positive regulation by small RNAs and the role of Hfq." *Proceedings of the National Academy of Sciences of the United States of America*, vol. 107, no. 21, pp. 9602–9607, 2010.

[6] J. Shine and L. Dalgarno, "Identical 3'-terminal octanucleotide sequence in 18S ribosomal ribonucleic acid from different eukaryotes. A proposed role for this sequence in the recognition of terminator codons." *The Biochemical journal*, vol. 141, no. 3, pp. 609–615, 1974.

[7] R. Lutz and H. Bujard, "Independent and tight regulation of transcriptional units in escherichia coli via the LacR/O, the TetR/O and AraC/I1-I2 regulatory elements," *Nucleic Acids Research*, vol. 25, no. 6, pp. 1203–1210, 1997.

[8] A. Jaramillo, "Predicitve Modelling of Riboregulatory Circuits to Re-engineer Living Cells." [Online]. Available: http://www2.warwick.ac.uk/fac/sci/wcpm/seminars/wcpm_seminar_presentation_alfonso_jaramillo.pdf

[9] A. Jaramillo, B. Kisov, and S. Shen, "Jaramillo Lab, unpublished data."

[10] Uri Alon, *An Introduction to Systems Biology*, 1st ed.

[11] G. L. Hersch, T. a. Baker, and R. T. Sauer, "SspB delivery of substrates for ClpXP proteolysis probed by the design of improved degradation tags." *Proceedings of the National Academy of Sciences of the United States of America*, vol. 101, no. 33, pp. 12 136–12 141, 2004.

[12] D. Brewer, M. Barenco, R. Callard, M. Hubank, and J. Stark, "Fitting ordinary differential equations to short time course data." *Philosophical transactions. Series A, Mathematical, physical, and engineering sciences*, vol. 366, no. 1865, pp. 519–544, 2008.

[13] C. G. Moles, P. Mendes, and J. R. Banga, "Parameter Estimation in Biochemical Pathways: A Comparison of Global Optimization Methods," *Genome Research*, pp. 2467–2474, 2003.

[14] C. Y. Hu, J. Varner, and J. B. Lucks, "Generating effective models and parameters for RNA genetic circuits," *ACS Synthetic Biology*, p. 150605124221004, 2015. [Online]. Available: http://pubs.acs.org/doi/abs/10.1021/acssynbio.5b00077

[15] N. Hansen, "The CMA evolution strategy: A comparing review," *Studies in Fuzziness and Soft Computing*, vol. 192, no. 2006, pp. 75–102, 2006.

[16] ——, "The CMA evolution strategy: A tutorial," *Vu le*, pp. 1–34, 2011. [Online]. Available: http://www.lri.fr/~hansen/cmatutorial110628.pdf

[17] K. a. P. Mclean and K. B. Mcauley, "Mathematical modelling of chemical processes-obtaining the best model predictions and parameter estimates using identifiability and estimability procedures," *Canadian Journal of Chemical Engineering*, vol. 90, no. 2, pp. 351–366, 2012.

[18] K. Z. Yao, B. M. Shaw, B. Kou, K. B. McAuley, and D. W. Bacon, "Modeling Ethylene/Butene Copolymerization with Multisite Catalysts: Parameter Estimability and Experimental Design," *Polymer Reaction Engineering*, vol. 11, no. 3, pp. 563–588, 2003.

[19] J. Beck, *Parameter Estimation in Engineering and Science*, 1st ed. Wiley, 1977.

[20] J. E. Jiménez-Hornero, I. M. Santos-Dueñas, and I. García-García, "Structural identifiability of a model for the acetic acid fermentation process," *Mathematical Biosciences*, vol. 216, no. 2, pp. 154–162, 2008.

[21] M. Grewal and K. Glover, "Identifiability of linear and nonlinear dynamical systems," *IEEE Transactions on Automatic Control*, vol. 21, no. 6, pp. 833–837, 1976.

[22] K. a. P. McLean, S. Wu, and K. B. McAuley, "Mean-squared-error methods for selecting optimal parameter subsets for estimation," *Industrial and Engineering Chemistry Research*, vol. 51, no. 17, pp. 6105–6115, 2012.

[23] J. J. Jitjareonchai, P. M. Reilly, T. a. Duever, and D. B. Chambers, "Parameter Estimation in the Error-in-Variables Models Using the Gibbs Sampler," *Canadian Journal of Chemical Engineering*, vol. 84, no. February, pp. 125–138, 2006.

[24] C. Andrieu, N. De Freitas, A. Doucet, and M. I. Jordan, "An introduction to MCMC for machine learning," *Machine Learning*, vol. 50, no. 1-2, pp. 5–43, 2003.

[25] J. B. Andersen, C. Sternberg, L. K. Poulsen, S. P. Bjø rn, M. Givskov, and S. r. Molin, "New unstable variants of green fluorescent protein for studies of transient gene expression in bacteria," *Applied and Environmental Microbiology*, vol. 64, no. 6, pp. 2240–2246, 1998.

[26] R. Iizuka, M. Yamagishi-Shirasaki, and T. Funatsu, "Kinetic study of de novo chromophore maturation of fluorescent proteins," *Analytical Biochemistry*, vol. 414, no. 2, pp. 173–178, 2011. [Online]. Available: http://dx.doi.org/10.1016/j.ab.2011.03.036

APPENDIX A
INITIAL EXPERIMENTAL DATA

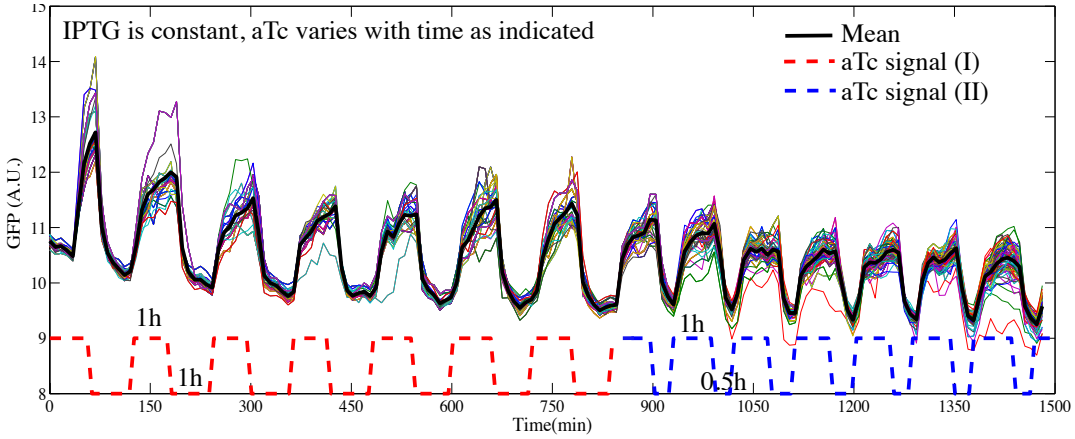

Fig. A.1: The *13_9* dataset, with aTc forcing shown. IPTG concentration is constant at a level which saturates the cell's response. Note the forcing curve's height is schematic - aTc concentation is switched between off, and a level which saturates the cell's response

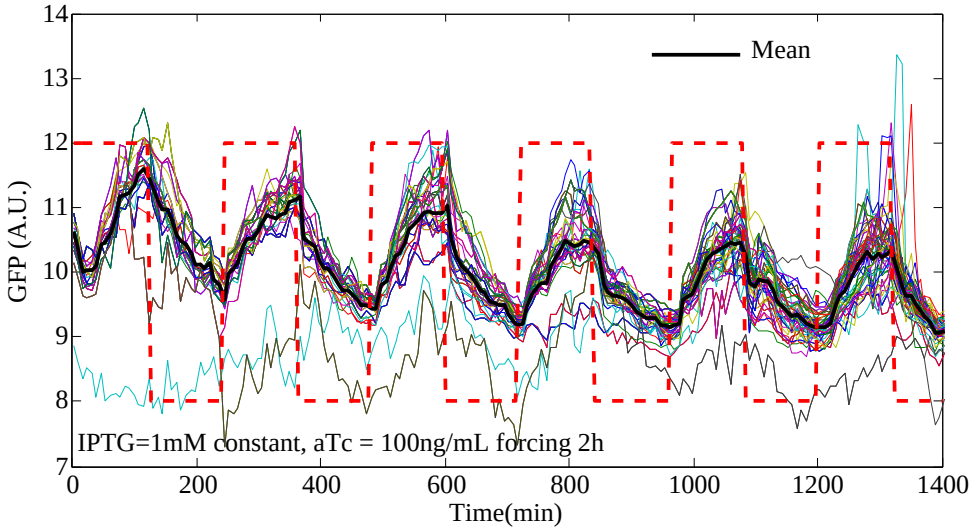

Fig. A.2: The *14_7* dataset, with aTc forcing shown. IPTG concentration is constant at a level which saturates the cell's response. Note the forcing curve's height is schematic - aTc concentation is switched between off, and a level which saturates the cell's response

APPENDIX B
PARAMETER LITERATURE REVIEW, AND ROUGH INITIAL PARAMETER BOUNDS

TABLE III: Literature references, or initial rough bounds, on parameter values, with those to be estimated shown in bold

Parameter	Value	Definition	Reference	Initial Bounds
N	300	Number of copies of promoter existing on plasmid DNA	Experimentally set	
z_0	9 AFU	Baseline experimental fluorescence	Experimentally determined	
α_L	11 nM/min	Maximal transcription rate of $P_{\mathrm{LlacO}-1}$ promoter	[7]	
α_T	11 nM/min	Maximal transcription rate of $P_{\mathrm{LtetO}-1}$ promoter	[7]	
f_L	620	Unitless ratio between repressed and unrepressed $P_{\mathrm{LlacO}-1}$ transcription rate	[7]	
f_T	2535	Unitless ratio between repressed and unrepressed $P_{\mathrm{LtetO}-1}$ transcription rate	[7]	
δ_g	0.0005 /min	GFP degradation rate	[25]	
γ	0.132 /min	GFP maturation rate	[26]	
v_z	100 nM/min	degradation constant of clpx	[11]	
K_z	75 nM/min	Dissociation constant of clpx	[11]	
$\boldsymbol{\Theta}$	nM/AFU	Ratio between GFP concentration and observed fluorescence		300 - 1000
$\boldsymbol{\mu}$	/min	Dilution rate		0.001-0.05
$\boldsymbol{\delta_m}$	/min	mRNA degredation rate		1 - 10^5
$\boldsymbol{\delta_s}$	/min	sRNA degredation rate		1 - 10^3
δ_{sm}	/min	Unstable sRNA:mRNA degradation rate		Set to δ_m
δ_c	/min	Stable sRNA:mRNA degradation rate		Set to δ_m
$\boldsymbol{k_{on}}$	/min	sRNA:mRNA binding rate		100 - 10^7
$\boldsymbol{k_{off}}$	/min	sRNA:mRNA unbinding rate		1 -10^8
$\boldsymbol{k_{hyb}}$	/min	sRNA:mRNA hybridization rate		1 - 10^4
$\boldsymbol{\beta}$	/min	Baseline translation rate of repressed mRNA		0.0001 - 10
$\boldsymbol{f_s}$		Ratio of repressed mRNA to unrepressed complex translation rate.		0.1 - 10^4

APPENDIX C
ADDITIONAL INITIAL RESULTS FIGURES

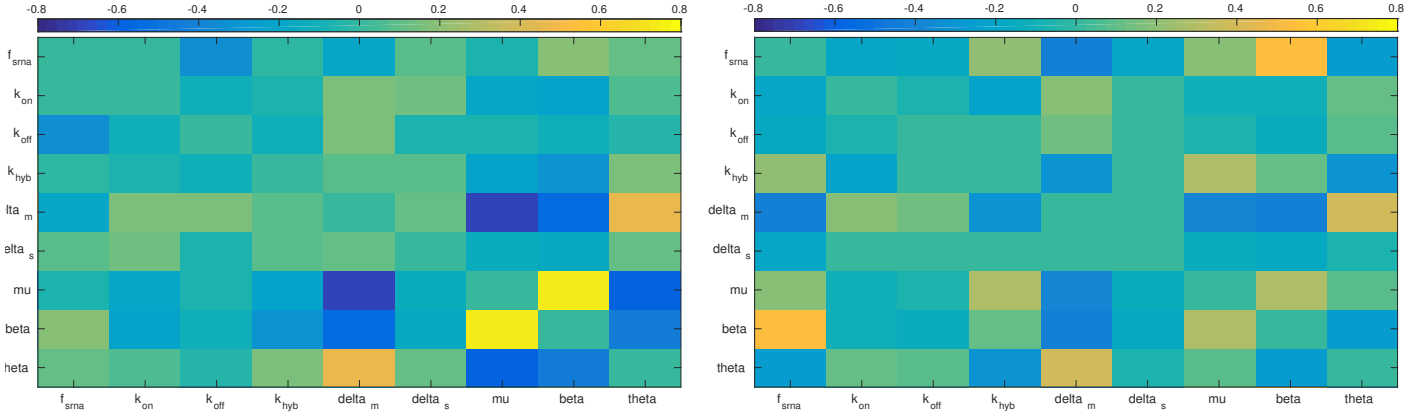

(a) Correlation matrix of estimated parameter sets, from the *13_9* dataset. **(b)** Correlation matrix of estimated parameter sets, from the *14_7* dataset.

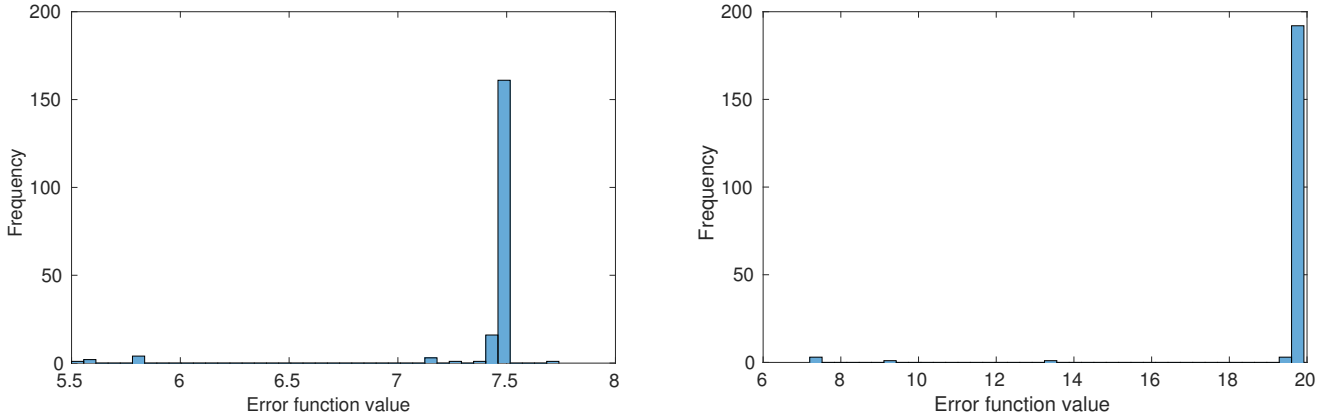

(c) Error values found from 200 initial parameter estimates, *13_9 dataset*. **(d)** Error values found from 200 initial parameter estimates, *14_7 dataset*

Fig. C.1: Inter-parameter correlation values and error function values, found from 200 initial parameter estimates, for the *13_9* and *14_7* datasets.

APPENDIX D
INITIAL PARAMETER ESTIMATES, FIT USING BOTH DATASETS

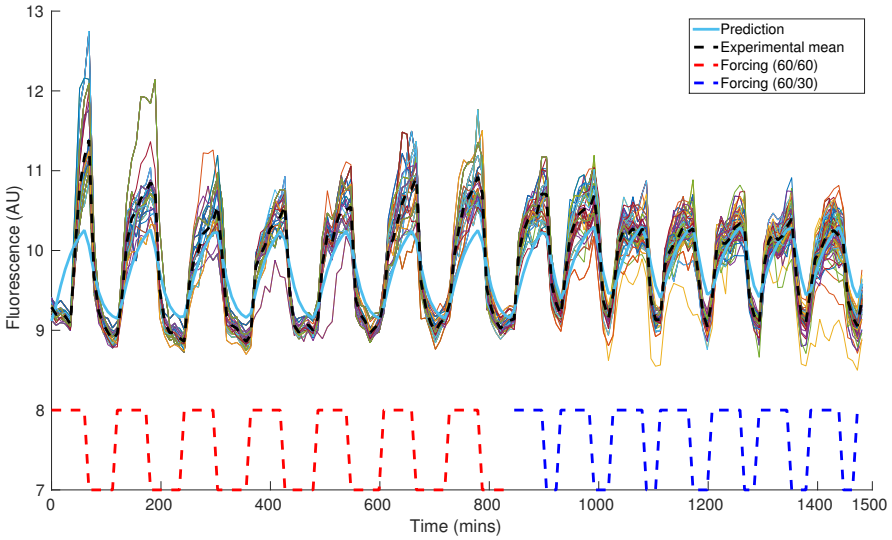

(a) Model prediction from the parameter set which gives lowest error when trained on the combination of both datasets, plotted against the *13_9* dataset.

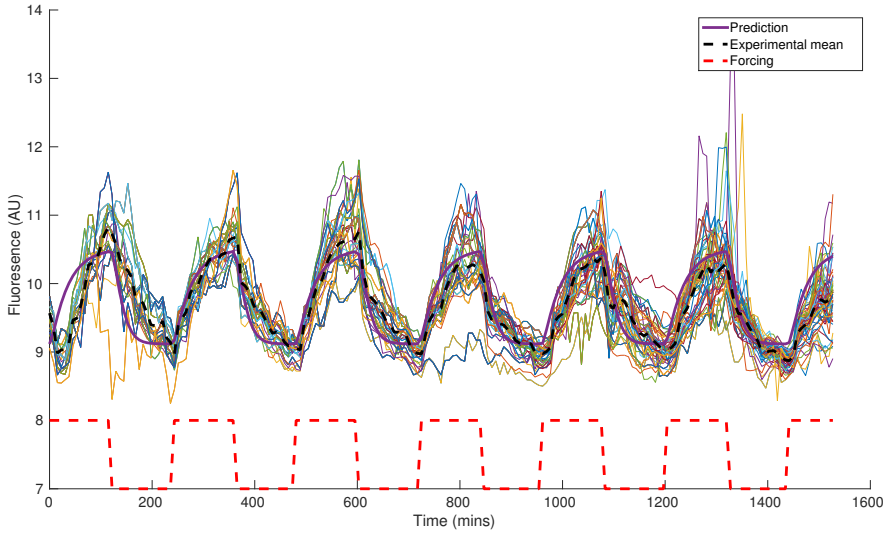

(b) Model prediction from the parameter set which gives lowest error when trained on the combination of both datasets, plotted against the *14_7* dataset.

Fig. D.1

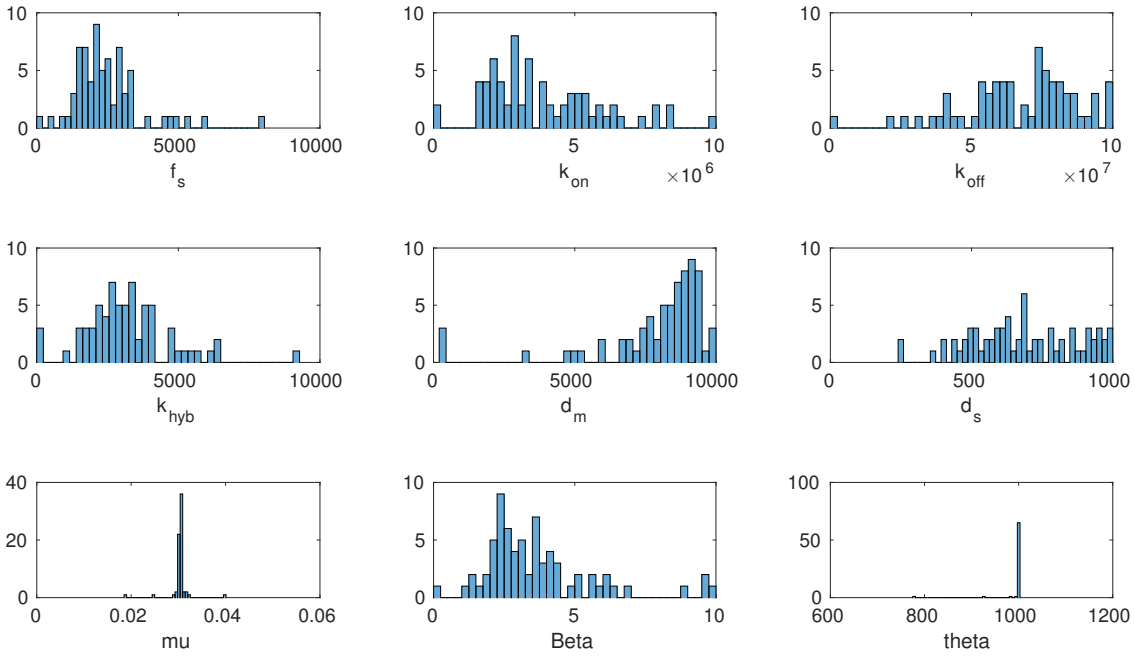

Fig. D.2: Histograms of estimated parameter values, found from 100 runs of the CMA-ES algorithm. Fitted to both the *13_9* and *14_7* datasets.

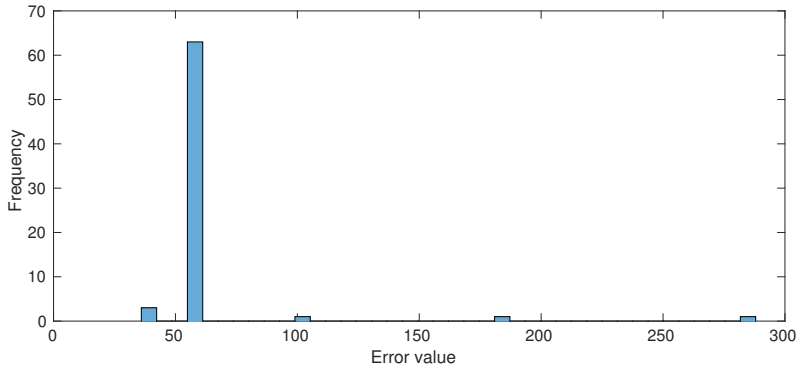

Fig. D.3: Error values found from 100 initial parameter estimates. Fitted to both the *13_9* and *14_7* datasets.

APPENDIX E
MODEL FIXED POINT

$$m = \frac{1}{2k_{\text{on}}\left(\mu+\delta_m\right)\left(k_{\text{hyb}}+\delta_m\right)}\left(\sqrt{2(\text{am}+\text{as})k_{\text{on}}\left(\mu+\delta_m\right)\left(\mu+\delta_s\right)\left(k_{\text{hyb}}+\delta_m\right)\left(k_{\text{hyb}}+k_{\text{off}}+\delta_m\right)+(\text{am}-\text{as})^2k_{\text{on}}^2\left(k_{\text{hyb}}+\delta_m\right)^2+\left(\mu+\delta_m\right)^2\left(\mu+\delta_s\right)^2\left(k_{\text{hyb}}+k_{\text{off}}+\delta_m\right)^2}\right. \tag{15}$$
$$\left.-(\text{am}-\text{as})k_{\text{on}}\left(k_{\text{hyb}}+\delta_m\right)+\left(\mu+\delta_m\right)\left(\mu+\delta_s\right)\left(k_{\text{hyb}}+k_{\text{off}}+\delta_m\right)\right)$$

$$c = \frac{k_{\text{hyb}}}{2k_{\text{on}}\left(\mu+\delta_m\right)\left(k_{\text{hyb}}+\delta_m\right)^2}\left(\sqrt{2(\text{am}+\text{as})k_{\text{on}}\left(\mu+\delta_m\right)\left(\mu+\delta_s\right)\left(k_{\text{hyb}}+\delta_m\right)\left(k_{\text{hyb}}+k_{\text{off}}+\delta_m\right)+(\text{am}-\text{as})^2k_{\text{on}}^2\left(k_{\text{hyb}}+\delta_m\right)^2+\left(\mu+\delta_m\right)^2\left(\mu+\delta_s\right)^2\left(k_{\text{hyb}}+k_{\text{off}}+\delta_m\right)^2}\right. \tag{16}$$
$$\left.+(\text{am}+\text{as})k_{\text{on}}\left(k_{\text{hyb}}+\delta_m\right)+\left(\mu+\delta_m\right)\left(\mu+\delta_s\right)\left(k_{\text{hyb}}+k_{\text{off}}+\delta_m\right)\right)$$

APPENDIX F
FIXED POINT SCATTERPLOT

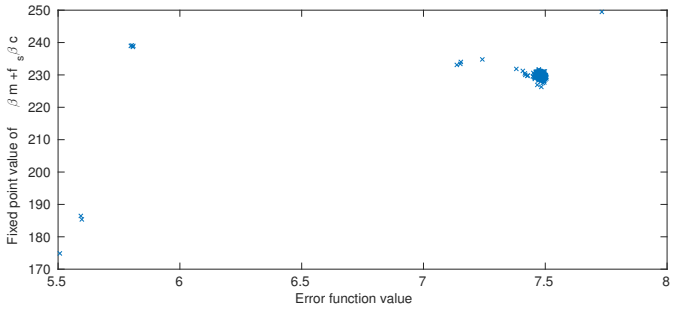

Fig. F.1: A scatterplot of the fixed point value of $\beta m + f_s\beta c$, for a given parameter set, against the error value of that set.

APPENDIX G
SIMPLIFIED MODEL ADDITIONAL RESULTS

TABLE IV

TABLE V: Initial bounds on parameters to be estimated in the simplified model, eq. (12) - eq. (14).

Parameter	Units	Definition	Initial Bounds
μ	/min	Dilution rate	0.001-0.1
F	nM /min	Phenomenological forcing	10-1500
Θ	nM/AFU	Ratio between GFP concentration and observed fluorescence	100 - 10000

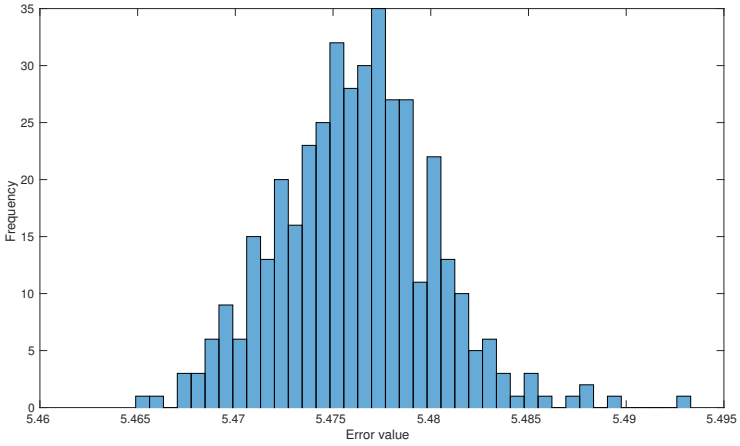

Fig. G.1